Desalination and Water Treatment
www.deswater.com
doi: 10.5004/dwt.2022.29033

277 (2022) 251–265
November

New eco-friendly FeS-modified biochar derived from peanut shells and walnut shells: a green synthesis approach for removal of lead

Renrong Liu[a,†], Qian Chen[a,†], Haixin Xia[a,†], Qi Zhong[a], XinYu Ren[a], Yichan Zhang[b], Yaohong Zhang[a,*], Hai Wang[a,c,*]

[a]*School of Life Science, School of Chemistry and Chemical Engineering, Zhejiang Key Laboratory of Alternative Technologies for Fine Chemicals Process, Shaoxing University, Shaoxing 312000, Zhejiang, China, emails: zhangyhsxu@126.com (Y.H. Zhang), wanghai@usx.edu.cn/wanghai2243@126.com (H. Wang), 1124131057@qq.com (R.R. Liu), 1970594446@qq.com (Q. Chen), 1650444758@qq.com (H.X. Xia), 2500745312@qq.com (Q. Zhong), 3486155056@qq.com (X.Y. Ren)*
[b]*Department of Chemistry and Chemical Engineering, Yancheng Institute of Technology, Yancheng 224051, Jiangsu, China, email: 1549635007@qq.com (Y.C. Zhang)*
[c]*Jianhu Provincial Wetland Park Management Committee, Shaoxing 312000, Zhejiang, China*

Received 2 June 2022; Accepted 13 October 2022

ABSTRACT

The study aimed at firstly preparing two eco-friendly biomaterials of PFeS&PEB and PFeS&WAB from peanut shells biochar (PEB) and walnut shells biochar (WAB) by loading with ferrous sulfide powder (Powder-FeS) to evaluate the ability to remove Pb(II) from sewage. FeS was immobilized to the surfaces biochar through functional groups such as –OH, –COOH and C–O. The results of batch experiments showed that PFeS&PEB had the maximum adsorption capacity (98.039 $mg \cdot g^{-1}$) when pH = 5 and the dosage was 0.75 $g \cdot L^{-1}$. The adsorption data were adequately simulated with adsorption kinetics and isothermal thermodynamic analysis, suggesting that the adsorption of Pb(II) by PFeS&PEB and PFeS&WAB was mainly monolayer chemisorption, and the adsorption process was spontaneous endothermic. The removal of Pb(II) was achieved by the association of complexation, redox, ion exchange, electrostatic attraction and physical adsorption. Reusability studies showed that PFeS&PEB and PFeS&WAB had good stability over four consecutive cycles. Hence, the cost-effective materials of PFeS&PEB and PFeS&WAB can be used as effective bio-adsorbent for the removal Pb(II) from wastewater.

Keywords: Biomaterial; Pb(II); Low-cost adsorbent; Sorption; Ion exchange

1. Introduction

Due to the rapid progress of industrialization and urbanization, a great amount of sewage containing Pb(II) from industries of mining and smelting as well as the fields of gasoline, electroplating, batteries and lead bombs was inevitably produced and discharged into natural environment, which consequently brought tremendous pressure and severe crises to the environment [1–3]. In addition, upon entering human body through food chain and water [4], Pb(II) might pose significant threats to human health, such as poisoning, anemia, neurological disorders, cancer, as well as bone, kidney and immune system damage, and even death [5,6]. Moreover, even trace amounts of Pb(II) was continuously discharged into nature will lead to Pb(II) accumulation/pollution, which subsequently would cause great harm to the health of human beings and ecological environment [7]. Therefore, Pb(II) wastewater should be properly treated before being released into the environment.

* Corresponding authors.
† These authors are co-first authors.

1944-3994/1944-3986 © 2022 Desalination Publications. All rights reserved.

The existing strategies for treating Pb(II)-containing wastewater include chemical precipitation [8], ion exchange [9,10], electrochemical method [11,12], and adsorption [13,14]. However, the first three processes cannot be widely applied in wastewater treatment because of complex manipulation, the second pollution and high investment [15–17]. Nevertheless, adsorptions have attracted extensive attention on account of its advantages of environmental friendliness, low prices and high efficiency together with facile operation [18–20]. As a common adsorbent, biochar was derived from waste biomass under anaerobic conditions at high temperature, which has been extensively applied in the elimination of heavy metals from sewage due to its superiorities of low price, facile preparation, numerous functional groups and easy availability of precursor sources [21,22]. However, the poor adsorption performance and difficult separation from solid-liquid mixtures limited its application in sewage treatment [23,24]. Hence, various composites have been prepared from biochar and other materials to improve the efficiency of biochar to absorb heavy metals, such as magnetic biochar [25,26], graphene@biochar [27], nano-Fe^0@biochar [28,29] and Fe–Mn modified biochar [30]. The study found that Fe–Mn modified biochar improved Pb(II) removal in water and soil by enhancing ion exchange and electrostatic attraction [30]. Cheng et al. [31] prepared new biochar using crofton weed and 1,3-diaminoguanidine monohydrochloride, enhanced its ability to adsorb Pb(II) in solution.

A large amount of Fe(II) ions and S(-II) ions provided by FeS can effectively stabilize divalent metals (Co(II), Cu(II), Ni(II), Mg(II), etc.) because of their surface chemistry and unique molecular structure. In addition, Fe(II) ions and S(-II) ions can produce good reducibility to facilitate heavy metal reduction because they can work as effective electron donors. Furthermore, FeS was an efficient scavenger that has been gradually used in the removal of heavy metals in soil and water, such as natural FeS minerals have been applied for the elimination of Cr(VI) ions in solution and the results demonstrated that natural FeS minerals displayed greater removal ability [32]. Moreover, FeS had the merits of low price, easy preparation and without secondary pollution. As a result, they can be used in the amendment of contaminated water bodies and soil [33–35], but they have the disadvantage of poor stability and easy deactivation due to its easy agglomeration. Therefore, stabilization measures should be taken to reduce its agglomeration so as to increase its removal efficiency.

In addition, the type of feedstock and combined composites of biochar had a great effect on its structure and adsorption efficiency [13]. Herein, peanut shells biochar (PEB) and walnut shells biochar (WAB) prepared at 450°C were selected as primitive biochar, two new bio-materials (PFeS&WAB and PFeS&PEB) were firstly prepared and their effectiveness for the elimination of Pb(II) were tested (Fig. 1). The main objectives were to: (1) prepare two new bio-materials (PFeS&WAB and PFeS&PEB); (2) study the performance and construction of PFeS&WAB and PFeS&PEB through microscopic technologies; (3) test the adsorption capacity of PFeS&WAB and PFeS&PEB for Pb(II) in simulated

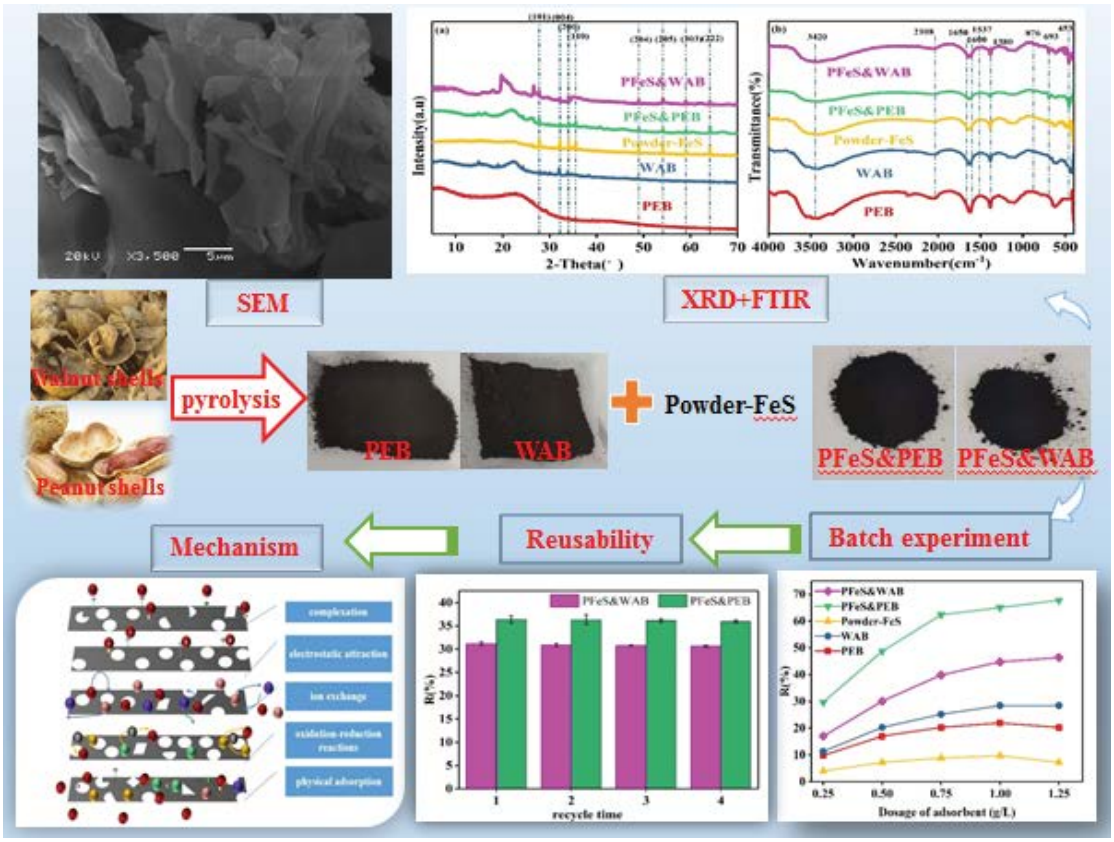

Fig. 1. Preparation of PEB, WAB, Powder-FeS, PFeS&PEB and PFeS&WAB, and removal Pb(II) in sewage.

sewage and (4) study the possible adsorption mechanism. This research provided a new idea for the ecological utilization of agricultural waste and offered a green, effective and economic environmental pollution clean-up for Pb(II) wastewater.

2. Materials and methods

2.1. Chemicals

All chemicals employed in the study were analytical grade (Powder-FeS, Sinopharm Chemical Reagent Co., Ltd., NaOH & HCl, Shanghai Aladdin Biochemical Technology Co., Ltd.). Peanut shells and walnut shells were purchased from the agricultural market of Zhumadian (Henan, China.). The anaerobic deionized water was produced by charging N_2 into deionized water for more than 30 min under stirring.

2.2. Preparation of adsorbents

Peanut shells and walnut shells were washed three times with deionized water and then heated in an oven at 120°C for 24 h. Subsequently, the resulting dried peanut shells and walnut shells were crushed into 1–2 cm pieces and carbonized in a muffle furnace at 450°C for 2 h. After that, the biochar was pulverized and sieved through a 60-mesh sieve at room temperature. Thus, the original peanut shell biochar (PSB) and walnut shell biochar (WAB) were successfully prepared.

In the study, the biochar (10 g) carbonized at 450°C was firstly dispersed in deionized water to make a suspension (10 g biochar/100 mL deionized water), and then Powder-FeS (10 g) was added with a 1:1 ratio to the above mixture and stirred at room temperature for 2 h, and then stood for 24 h. After centrifuged at 8,000 rpm, dried at 65°C, peanut shells biochar & Powder-FeS (PFeS&PEB) and walnut shells biochar & Powder-FeS (PFeS&WAB) were obtained for the study.

2.3. Characterization of adsorbents

The surface morphology and elemental distribution of PEB, WAB, Powder-FeS, PFeS&PEB and PFeS&WAB were observed with scanning electron microscopy-Energy-dispersive X-ray spectroscopy (SEM-EDS; JEOL 6500F, Japan). Surface functional groups were investigated by Fourier-transform infrared spectroscopy (FTIR; Nexus 670, Thermo Nicolet, Madison) in the wave number range of 4,000–400 cm^{-1}. The crystalline structures of the adsorbents were identified by X-ray diffraction (XRD; D/Max-IIIA X-ray Diffractometer, Rigaku Corp., Japan) at a rate of about 5°min^{-1} (2θ = 5°–70°). The specific surface area and particle size distributions of PEB, WAB, PFeS&PEB and PFeS&WAB were tested by Brunauer–Emmett–Teller (BET, ASAP2460, USA). The surface composition of PFeS&PEB and PFeS&WAB was determined by X-ray photoelectron spectroscopy (XPS, Kratos AXIS Ultra DLD, Japan).

2.4. Adsorption experiments

The removal performance of PEB, WAB, Powder-FeS, PFeS&PEB and PFeS&WAB was investigated by a series of adsorption experiments. The effects of initial concentration of Pb(II) (20–100 $mg{\cdot}L^{-1}$), pH values (2–7), adsorbent dosage (0.25–1.25 $g{\cdot}L^{-1}$) and reaction time (0–270 min) on the removal performance of Pb(II) ions were investigated, respectively. Other variables used the following criteria: the adsorbent (0.075 g) was added to 100 mL of Pb(II) (60 $mg{\cdot}L^{-1}$) in a 250 mL Erlenmeyer flask. The flask was then sealed and shaken at 200 rpm under 25°C. Then the initial pH values of the solution were adjusted to 5 using 0.1 $mol{\cdot}L^{-1}$ NaOH or HCl. When equilibrium was achieved in the adsorption process, the adsorbent samples were centrifuged at 4,000 rpm for 15 min. The supernatant was collected through filtrations. Afterwards, the concentrations of Pb(II) in the residual solution were analyzed using UV-Vis spectrophotometry (Detailed methods were in supporting information). The removal rate (R) and the removal capacity (q_e) was calculated using Eqs. (1) and (2). The detailed of equations was in the supporting information. Meanwhile, blank control (no adsorbent) was used to refrain from the effect of precipitation in the process of adsorption in the experiment.

2.5. Reusability experiments

Adsorbent regeneration was an important way to reduce treatment cost, so the regeneration performance was one significant index to assess the pollution control ability of adsorbents. Since protonation of PFeS&WAB and PFeS&PEB surface functional groups was easy to occur in strongly acidic solutions, Pb(II) was released into the solution by H^+ substitution. Therefore, HNO_3 (0.1 M) was chosen as the eluent for Pb(II) desorption. PFeS&WAB (0.075 g) and PFeS&PEB (0.075 g) were added into a conical flask containing Pb(II) (100 mL, 60 $mg{\cdot}L^{-1}$), respectively, and the adsorption properties were determined after shaking at 200 rpm at 25°C for 240 min. Then, the adsorbed PFeS&WAB and PFeS&PEB were placed in a conical flask containing HNO_3 (100 mL 0.1 M), respectively, and oscillated at 200 rpm at 25°C for 240 min. After each desorption, washed with distilled water and dried in an oven at 65°C for the next cycle. The process was repeated four times to determine the repeatability and stability of PFeS&WAB and PFeS&PEB to remove Pb(II).

2.6. Regression analysis

According to the report of Hamdy et al. [36], a pure quadratic model was used to determine the influence of experimental factors on Pb(II) removal efficiency. The least square method was used to estimate the model parameters. The coefficient of determination (R^2) and adjusted R^2 (adjust-R^2) were used to estimate the accuracy of the model. Meanwhile, t-test was used to test the statistical significance of the model. All calculations were done using Matlab R2017b software.

3. Results and discussion

3.1. Characterization of adsorbents

SEM images (Fig. 2a) shows that PEB had lamellar structures and smooth surface. The main elements of EDS analysis (Fig. 2A) were C and O, which contained little K and

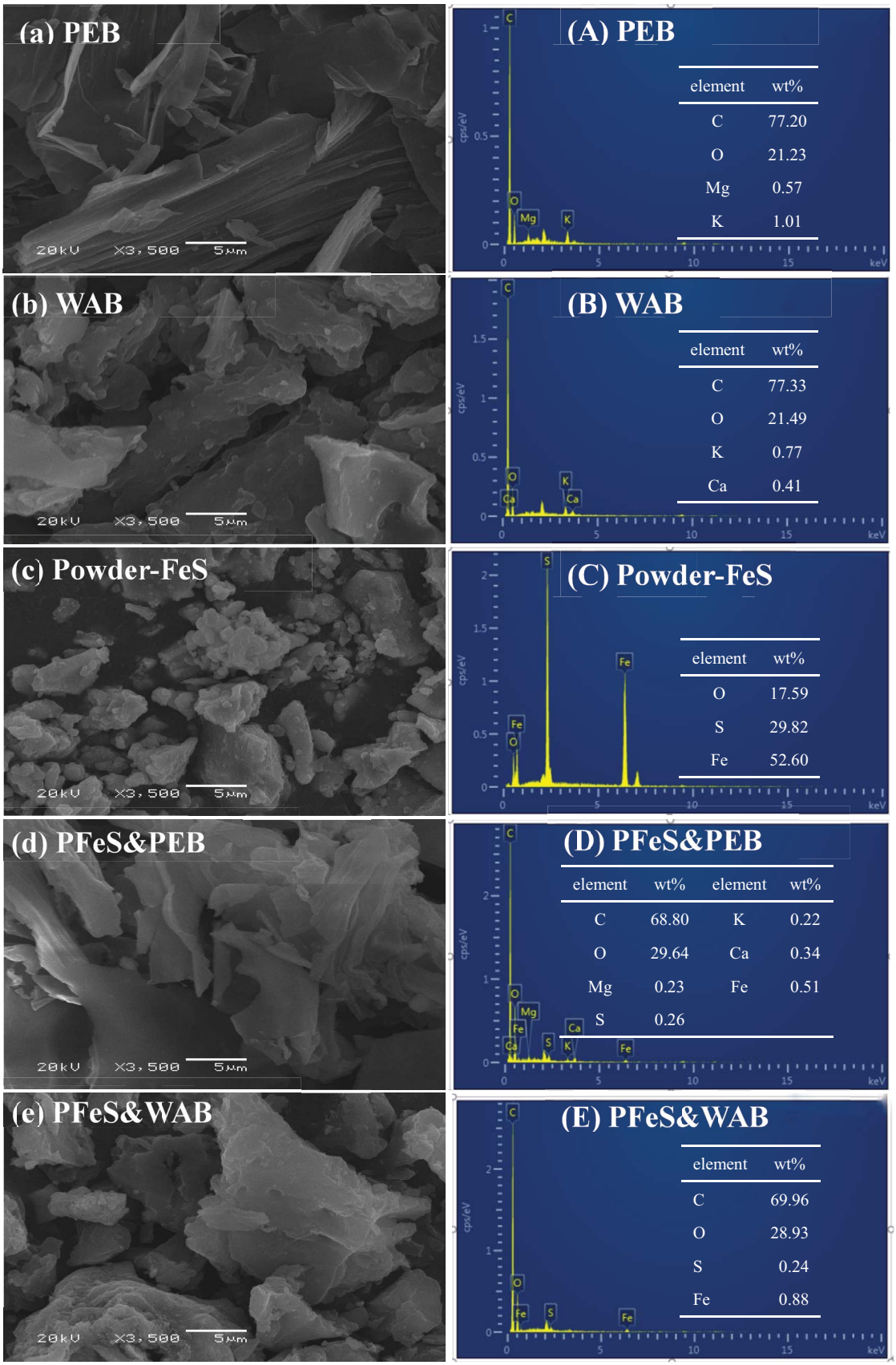

Fig. 2. SEM images and EDS spectrum of PEB (a, A), WAB (b, B), Powder-FeS (c, C), PFeS&PEB (d, D) and PFeS&WAB (e, E).

Mg. The WAB had rough surface with small bumps and pores (Fig. 2b). EDS analysis (Fig. 2B) showed that the main elements were similar to PEB except that Mg was replaced by Ca. The Powder-FeS was irregular clumps. The presence of oxygen indicated partial oxidation of Powder-FeS. After modification with Powder-FeS, small particles appeared on the surface of PFeS&PEB and PFeS&WAB (Fig. 2c and d). PFeS&PEB still showed obvious lamellar structure. However, the roughness of PFeS&WAB surface decreased obviously and showed a large distribution. Fig. 2D and E showed the presence of Fe and S on both PFeS&PEB and PFeS&WAB surfaces, indicating that FeS was successfully loaded onto the PEB and WAB surfaces. The lamellar structure of PEB and the rough surface structure of WAB were conducive to the adhesion of Powder-FeS.

The specific surface area and particle size distributions of PEB, WAB, PFeS&PEB and PFeS&WAB are listed in Table S1. As shown in Table S1, the specific surface area (S_{BET}) of PFeS&PEB and PFeS&WAB were 51.14 and 46.49 $m^2 \cdot g^{-1}$, respectively, which was higher than that of original biochar (PEB = 8.07 $m^2 \cdot g^{-1}$, WAB = 7.19 $m^2 \cdot g^{-1}$). The pore size and pore volume of PFeS&PEB and PFeS&WAB were 8.57 nm, 0.082 $cm^3 \cdot g^{-1}$, and 10.86 nm, 0.099 $cm^3 \cdot g^{-1}$, respectively. The results demonstrated that after modification with Powder-FeS, PFeS&PEB and PFeS&WAB had large surface areas and reduction in pore size, resulting in a higher porosity.

The XRD patterns of PEB, WAB, Powder-FeS, PFeS&PEB and PFeS&WAB are displayed in Fig. 3a. (101), (004), (200), (110), (204), (205), (303) and (222) corresponded to 27.28°, 32.21°, 34.03°, 35,58°, 48.97°, 54.09°, 59° and 64.09°, respectively [37]. They are characteristic peaks of FeS, and also they are appeared in the XRD of PFeS&PEB and PFeS&WAB, which indicated that FeS was successfully loaded on PFeS&PEB and PFeS&WAB surfaces. PEB and WAB showed characteristic diffraction peaks at 22° and large layer-to-layer distance (d-spacing). The large d-spacing was ascribed to C–O, O=C–O and –OH [38,39]. The characteristic peaks of PFeS&PEB and PFeS&WAB were observed, respectively, indicating PFeS&PEB and PFeS&WAB were modified by PEB and WAB.

The FTIR spectra of PEB and WAB before and after FeS modification are presented in Fig. 3b. The characteristic peak at 3,420 cm^{-1} represented –OH [40]. Compared with WAB and PEB, PFeS&PEB and PFeS&WAB had smaller –OH peaks, probably due to reactions with FeS. The band at 2,108 cm^{-1} was attributed to C=C–N [41], 1,650–1,600 cm^{-1} represented C=O and COOH [42], the bands at 1,537 cm^{-1} attributed to C=C on the benzene ring [43]. The peaks at 1,380 cm^{-1} for C–O–C and 876 cm^{-1} for C–H [44]. The band at 453 cm^{-1} was related to Fe–S [45]. The absorption peak appeared at 693 cm^{-1}, indicating the presence of Fe–O [41]. The characteristic peaks of –OH, C=C–N, C=O, COOH and C–O–C decreased significantly after loading FeS, and PFeS&PEB were more distinct than PFeS&WAB. It may be that there were more sites in PEB to react with FeS. The presence of peaks Fe–S and Fe–O suggested that FeS was loaded onto WAB and PEB by Fe–O, Fe–S and intermolecular forces.

The chemical composition and bonds of PFeS&PEB and PFeS&WAB were analyzed by XPS technique. Fe and S elements were detected in PFeS&PEB and PFeS&WAB, indicating that the material was successfully prepared. Fig. 4a shows the spectra of C1s orbital for PFeS&PEB. 283.56, 284.77 and 287.7 eV represented C–C, C–O, and C=O [46,47], respectively. Fig. 4b shows the O1s orbital spectra of PFeS&PEB, where 528.90, 530.29 and 531.61 eV corresponded to peaks of –OH, Fe–O and C=O [48–50], respectively. Fig. 4c shows the spectra of Fe 2p orbital of PFeS&PEB, 710.96, 718.28 and 724.91 eV corresponded to Fe(II), and Fe(III) [51,52], respectively. Moreover, Fe(II) had a higher peak area (66.36%), and the appearance of Fe(III) indicated that part of Fe(II) was oxidized. Fig. 4d shows the spectra of S 2p orbitals of PFeS&PEB,163.07 and 168 eV corresponded to Sn^{2-} (63.28%) and SO_4^{2-}(36.72%) [53,54], respectively. PFeS&WAB had the same C and O peaks (Fig. 4e and f) as PFeS&PEB, but the peaks were slightly offset (C–C: 283.52 eV, C–O: 284.82 eV, C=O: 287.59 eV, –OH: 529.01 eV, Fe–O: 530.15 eV, and C=O: 531.35 eV). The Fe 2p (Fig. 4g) and S 2p (Fig. 4h) orbitals of PFeS&WAB were significantly different from of PFeS&PEB. New peaks at 709.97, 711.92, 717.04 and 724.87 eV in Fe 2p corresponded to FeO, Fe(III), Fe(II) and Fe(III) [55–57], respectively.

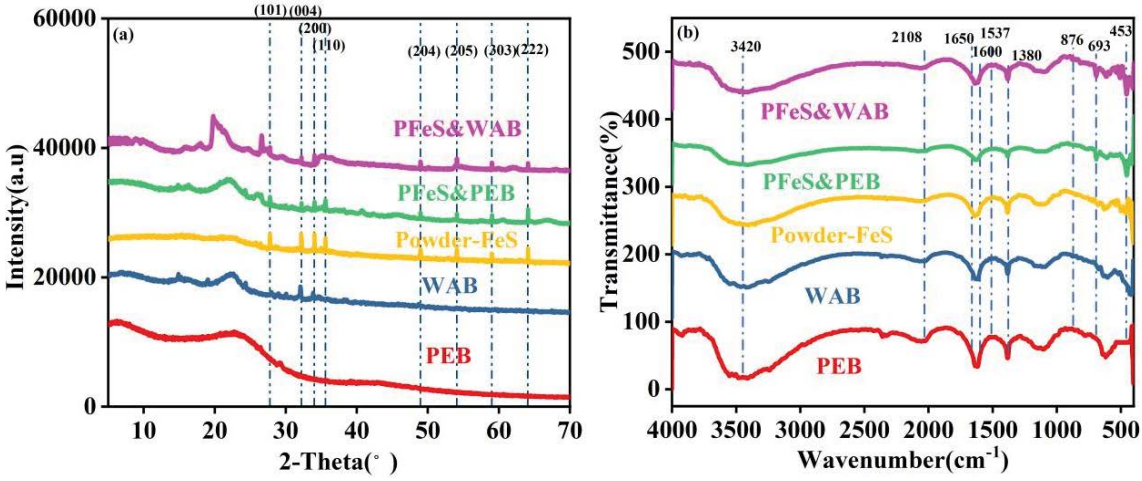

Fig. 3. XRD patterns (a) and FTIR spectra (b) of PEB, WAB, Powder-FeS, PFeS&PEB and PFeS&WAB.

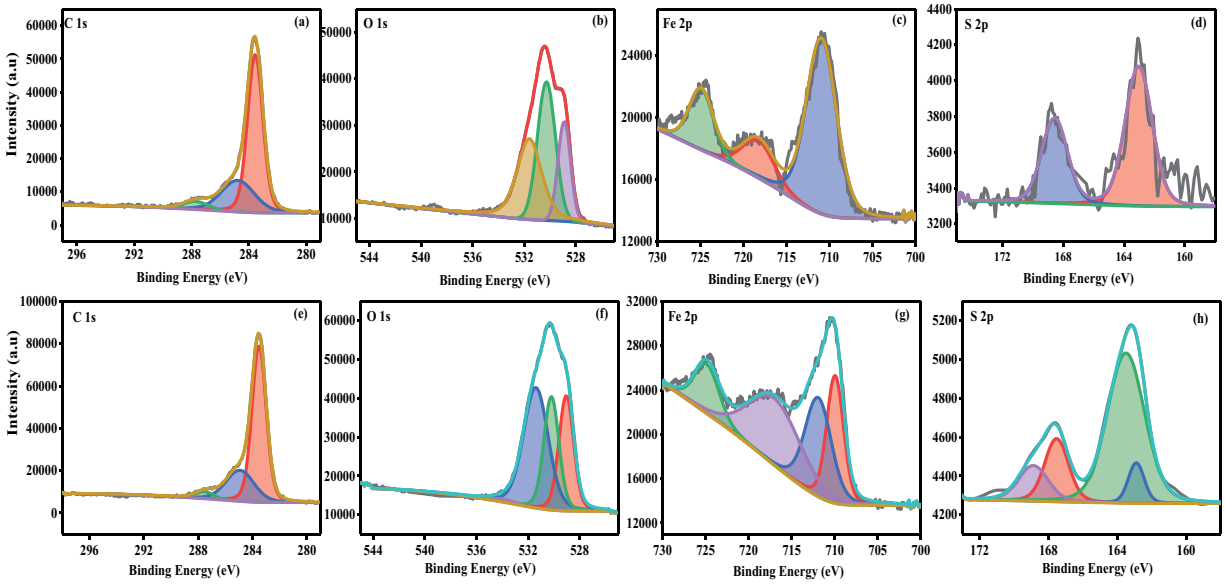

Fig. 4. XPS spectra of PFeS&PEB (a~d) and PFeS&WAB (e~h).

The peak area of Fe(II) (59.69%) was smaller than that of PFeS&PEB. New peaks at 162.9, 167.53, 163.5 and 168.88 eV appear in S2p corresponding to S–O, FeS_2, S^0 and SO_4^{2-} [53,55,58,59], respectively. Compared with PFeS&PEB and PFeS&WAB, PFeS&PEB contains higher Fe(II) and Sn^{2-}, so PFeS&PEB had higher stability.

3.2. Adsorption experiments

In order to assess the adsorption performance, the effects of various experimental parameters (contact time (0–270 min), pH (2–7), dosage of adsorbent (0.25–1.25 g·L^{-1}), initial concentration of Pb(II) (20–100 mg·L^{-1})) on the removal efficiency of Pb(II) were investigated.

As shown in Fig. 5a, the five materials showed the same trend. Removal increased rapidly at first, then decreased gradually, and finally reached adsorption equilibrium. The adsorption process can be roughly divided into three stages: 0–30 min rapid adsorption, 30–210 min slow adsorption, 210 min after the equilibrium stage. At the beginning of the reaction, many active sites were available on the surface of the adsorbent, and Pb(II) rapidly bound to the adsorbent. With the increase of time, the surface active sites of adsorbent were occupied gradually, the adsorption efficiency decreased gradually, and the change of removal efficiency decreased. At 210 min, the surface active sites of the adsorbent were completely occupied and the adsorption equilibrium was reached [60]. As can be seen from Fig. 5a, when equilibrium was reached, the removal efficiency PFeS&PEB (37.982%) > PFeS&WAB (31.321%) > WAB (26.590%) > PEB (21.805%) > Powder-FeS (12.289%).

The pH is an important parameter affecting the removal efficiency of adsorbent. It can change the surface charge distribution and functional group dissociation of adsorbent. In Fig. 5b, the removal rates (*R*) of the five materials displayed the same trend that increased first and then decreased. The removal efficiencies of PEB, WAB, Powder-FeS, PFeS&PEB and PFeS&WAB increased from 9.509%, 12.207%, 2.250%, 16.557% and 12.207% to 25.802%, 30.288%, 11.258%, 45.241% and 37.085%, respectively. At pH = 5, all five materials had the maximum removal efficiencies. PFeS&PEB had the highest removal efficiency (45.24%). It was demonstrated that the state of oxygen-containing groups (such as –OH and –COOH) on the surface of biochar materials was easily affected by solution pH [61]. Superficial –OH and –COOH of the five adsorbents were proved by XRD, XPS and FTIR. Wherefore, the large number of H^+ in the acidic aqueous solution prevented the deprotonation of the oxygen-containing group (–OH and –COOH), leading to a weakened electrostatic attraction to Pb(II) [62]. At the same time, a large amount of H^+ in solution had a strong competitive effect with Pb(II), which made the adsorptive property of the materials to Pb(II) decreased [63]. With the increased of pH, the concentration of H^+ in the solution gradually decreased, and the competition for Pb(II) was weakened. At the same time, the oxygen-containing functional groups on the surface of the adsorbent dissociated, the number of negative charges on the surface of the adsorbent increased, and the electrostatic attraction increased. When pH = 5, it had the maximum value, which might be caused by the maximum dissociation of functional groups on the surface of the adsorbent [13].

The zero charge point of pH (PZC) was an important indicator of the surface charge state of adsorbent. The detailed description of determination of PZC was in the supporting information. The PZC of PEB, WAB, and Powder-FeS were all greater than 5, while PFeS&PEB and PFeS&WAB were all less than 5 in Fig. 6. The surface of the adsorbent was negatively charged when $\Delta pH < 0$ [64]. The electrostatic attraction immobilized the positively charged Pb(II) in the solution to the surface of the adsorbent [65]. Therefore, PFeS&PEB and PFeS&WAB had high removal rates. In addition, at a low pH value, many H^+ competed with Pb(II) for active sites on the adsorbent surface. With

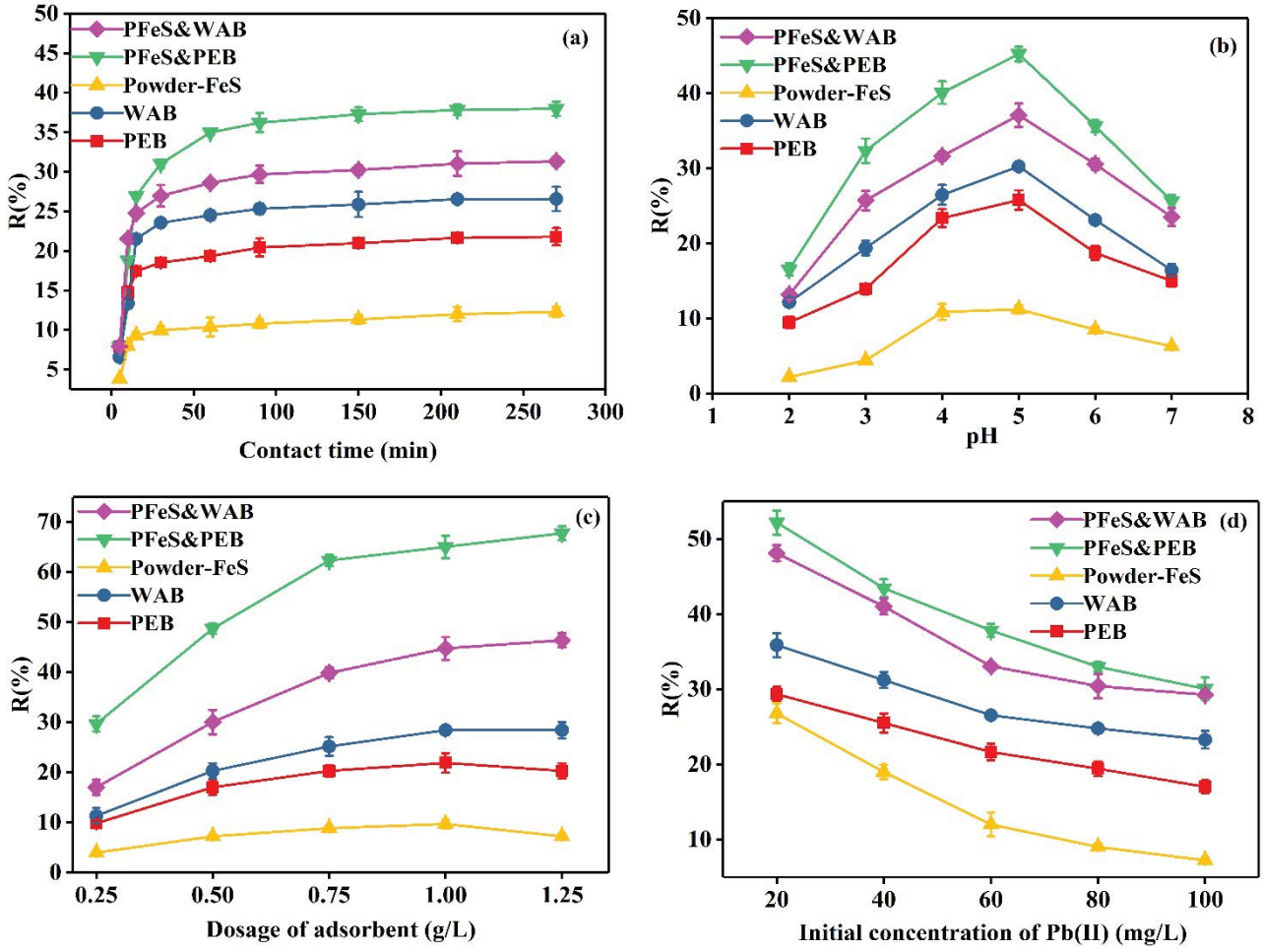

Fig. 5. Effect of contact time (a), pH (b), dosage of adsorbents and initial concentration of Pb(II) (d).

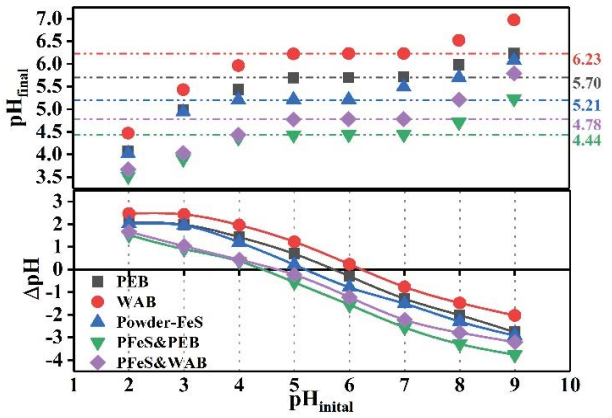

Fig. 6. Measurement of the pH of point of zero charge (PZC) of the materials (PEB, WAB, Powder-FeS, PFeS&PEB, and PFeS&WAB).

the increase of pH value, the concentration of H^+ in the solution gradually was decreased, the competitive effect was gradually weakened, and the removal efficiency was increased [66]. When ΔpH > 0, the surface of the adsorbent had positive charges, which generated electrostatic repulsion with Pb(II). However, it was calculated from the previous literatures that Pb(II) will form $Pb(OH)_2$ precipitation when pH = 5.8 [67]. As a result, the removal efficiency decreased with the decrease of Pb(II) concentration in the solution.

The dosage of adsorbent was a significant index affecting the removal rate. The optimal dosage can remove pollutants economically and efficiently. The influence of the dosage of five materials on the removal efficiency of Pb(II) are shown in Fig. 5c. The amount of adsorbent was positively correlated with the removal rate. PFeS&PEB had the highest removal rate (67.754%), followed by PFeS&WAB (46.394%) > WAB (28.450%) > PEB (20.293%) > Powder-FeS (7.243%). The optimal dosage was 0.75 $g{\cdot}L^{-1}$ because the rate of dosage change between 0.25 and 0.75 $g{\cdot}L^{-1}$ was significantly higher than 0.75–1.25 $g{\cdot}L^{-1}$. With the increase of dosage, the removal rate increased, because high dosage increased the number of active sites [68]. However, the change of removal rate gradually decreased, which may be due to the stacking of the active sites caused by the high dose of adsorbent, and the utilization efficiency of the active sites decreased. The result of this experiment was consistent with those of previous studies [69].

Fig. 5d shows the changes in the removal rate of the five sorbents under different initial Pb(II) concentrations. PFeS&PEB had the highest removal rate (52.202%), followed by PFeS&WAB (48.124%), WAB (35.889%), PEB (29.364%), and Powder-FeS (26.811%). As can be seen from Fig. 5d, the removal rate declined gradually with the increase of the initial concentration of Pb(II). The high concentration of Pb(II) raised the contact opportunity between the adsorbent and Pb(II), and improved the utilization rate of the surface active sites of the adsorbent. However, the adsorption sites on the surface of the adsorbent are limited. The adsorbent cannot fix free Pb(II) when all the adsorption sites were occupied. Therefore, the higher concentration of Pb(II), the more residual Pb(II) in the final solution, and the lower removal efficiency. The change of adsorption property of adsorbent before 60 mg·L^{-1} was more significant than that of after. Therefore, the initial Pb(II) concentration was selected as 60 mg·L^{-1} in further study.

3.3. Adsorption kinetics, adsorption isotherm and thermodynamics

To further explore adsorption performance and removal mechanism of the adsorbent, further study of kinetics (kinetic models of pseudo-first and pseudo-second), isothermal model (Langmuir and Freundlich) and thermodynamics were performed.

Two kinetic models were used for further analysis. Pseudo-first kinetic model and pseudo-second kinetic models are in Eqs. (3) and (4) of the supporting information.

Langmuir model (L-model) assumed that the biomaterial surface was uniform and the adsorption process was monolayer and directional. There was no interaction between the adsorbed particles. Freundlich model (F-model) assumed that the process was inhomogeneous multilayer physical adsorption. The adsorption equations of L-model and F-model are in Eqs. (5) and (6). The detailed of equations were in the supporting information.

To further investigate the influence of temperature on Pb(II) removal efficiency of biomaterial, Gibbs free energy, enthalpy change and entropy change were calculated by Eqs (7)–(9) of the supporting information.

Fitting figures of pseudo-first and second kinetic model are shown in Fig. 7a and b. The kinetics models parameters of pseudo-first and second kinetic model of Pb(II) on five sorbents are shown in Table 1. It can be observed from Fig. 7a and b and Table 1 that the correlation coefficient R^2 (PEB: 0.999, WAB: 0.999, Powder-FeS: 0.998, PFeS&PEB: 0.998, PFeS&WAB: 0.999) of the pseudo-second model were higher than that of pseudo-first model (R^2: PEB: 0.959, WAB: 0.905, Powder-FeS: 0.949, PFeS&PEB: 0.979, PFeS&WAB: 0.963). And the pseudo-second order q_e calculated value was closer to the real adsorption value $q_{e,exp}$.

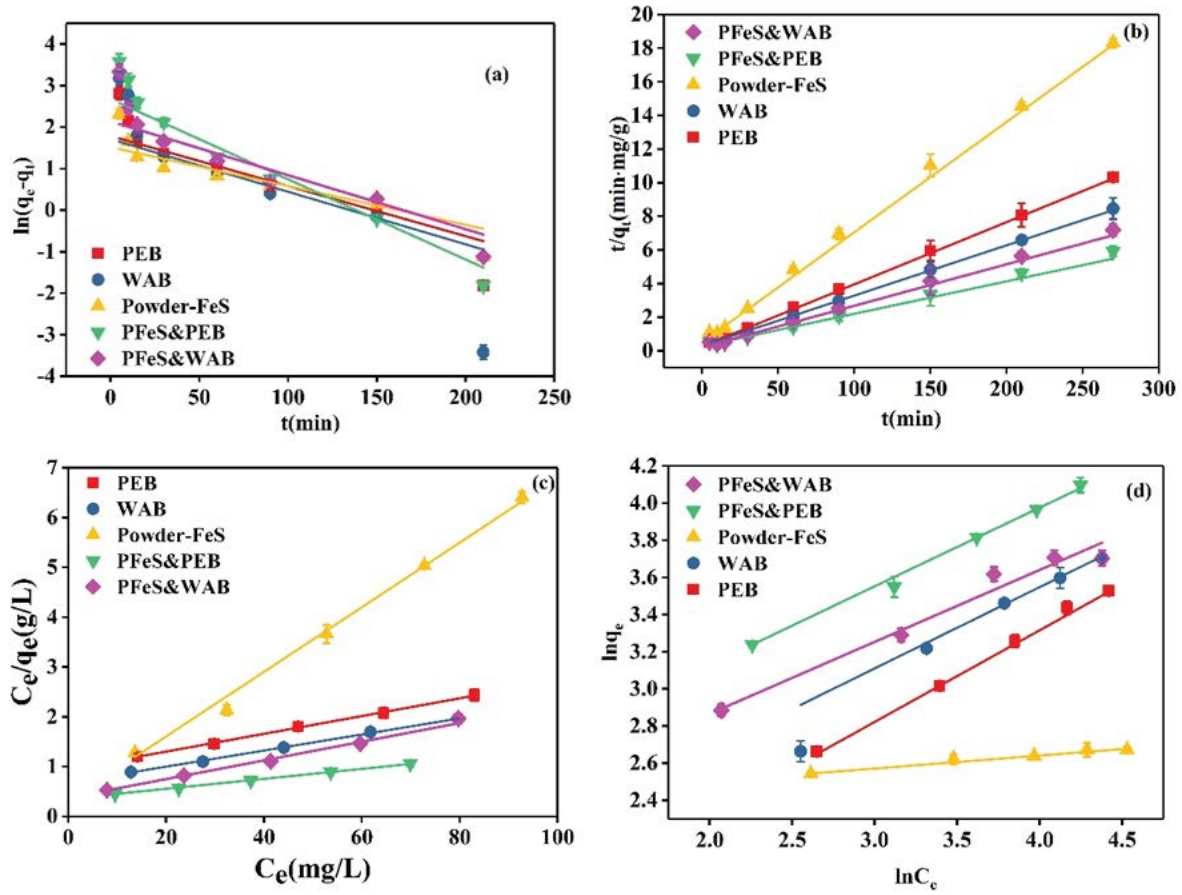

Fig. 7. Pseudo-first kinetic model (a), pseudo-second kinetic model (b), L-model (c) and F-model (d) study of Pb(II) adsorption by PEB, WAB, Powder-FeS, PFeS&PEB and PFeS&WAB.

Table 1
Adsorption kinetic and isotherm models parameters of Pb(II) adsorption with PEB, WAB, Powder-FeS, PFeS&PEB and PFeS&WAB

Absorbents		Pseudo-first kinetic model			Pseudo-second kinetic model			L-model			F-model	
	$q_{e,exp}$ (mg·g^{-1})	k_1 (min^{-1})	q_e (mg·g^{-1})	R^2	k_2 (g(mg·min)$^{-1}$)	q_e (mg·g^{-1})	R^2	R_L	q_m (mg·g^{-1})	K_L (L·mg^{-1})	R^2	K_F (L·mg^{-1})	1/n
PEB	26.166 ± 2.684	0.017	8.042 ± 0.145	0.959	0.006	26.738 ± 2.532	0.999	0.725	55.866 ± 4.685	0.019	0.998	2.467 ± 0.021	0.606
WAB	37.586 ± 4.053	0.025	12.548 ± 1.032	0.905	0.003	33.113 ± 3.783	0.999	0.647	57.803 ± 4.823	0.027	0.998	3.566 ± 0.053	0.567
Powder-FeS	14.747 ± 1.287	0.012	4.837 ± 0.023	0.949	0.007	15.038 ± 1.384	0.998	0.126	15.060 ± 1.975	0.345	0.995	10.705 ± 0.639	0.069
PFeS&PEB	45.579 ± 4.176	0.023	19.026 ± 2.258	0.979	0.002	47.847 ± 3.954	0.998	0.631	98.039 ± 8.469	0.029	0.996	9.342 ± 0.737	0.435
PFeS&WAB	31.909 ± 1.985	0.016	10.022 ± .1123	0.963	0.003	38.610 ± 2.746	0.999	0.612	59.524 ± 4.086	0.032	0.999	8.218 ± 0.597	0.383

The results demonstrated that chemisorption was dominant in the process of Pb(II) adsorption of the five materials, and the adsorption efficiency was related to the active sites on the surface of the adsorbent.

Fig. 7c and d are the fitting diagrams of L-model and F-model, respectively. Table 1 shows the relevant parameters of L-model and F-model. It is observed from Fig. 7c and d that the fitting effect of L-model was better. The correlation coefficient R^2 of L-model (R^2: PEB = 0.998, WAB = 0.998, Powder-FeS = 0.995, PFeS&PEB = 0.996, PFeS&WAB = 0.999) in Table 1 is greater than that of F-model (R^2: PEB = 0.988, WAB = 0.982, Powder-FeS = 0.972, PFeS&PEB = 0.995, PFeS&WAB = 0.969). The L-model can well describe the adsorption process of Pb(II) by adsorbent. The adsorption of Pb(II) by five adsorbents were monolayer. The R_L values of the five materials were all between 0 and 1, indicating that the adsorption of Pb(II) had a good adsorption process [70]. F-model parameter 1/n also ranged from 0 to 1, indicating that chemical reactions occurred during the adsorption process [71].

Therefore, the addition of Powder-FeS enhanced the adsorption properties of PEB and WAB, which may be due to its strong reducibility. The lower adsorption efficiency of PFeS&WAB compared with PFeS&PEB may be since FeS powder blocked the micropores on the WAB surface, resulting in a reduced surface area, which was not conducive to the physical adsorption of Pb(II). Although the microporous structure on the surface of PEB was not obvious, the rich lamellar structure was enough to load enough FeS, which not only avoided the excessive loss of surface area, but also was more favourable to the adsorption of Pb(II).

The relevant thermodynamic parameters of the five materials are presented in Table 2. $\Delta G < 0$ indicated that the adsorption process of Pb(II) can proceed spontaneously [72]. The change of ΔG was not obvious when the temperature increased, which indicated that the influence of temperature change on the process was not obvious.

Table 2
Thermodynamics parameters of PEB, WAB, Powder-FeS, PFeS&PEB and PFeS&WAB

Adsorbent	Temperature (°C)	ΔG (kJ·mol^{-1})	ΔH (kJ·mol^{-1})	ΔS (J·mol^{-1})
	25	–0.145		
PEB	35	–0.276	12.948	3.713
	45	–0.404		
	25	–0.988		
WAB	35	–1.110	12.877	2.851
	45	–1.246		
	25	–4.086		
Powder-FeS	35	–4.379	31.485	5.304
	35	–4.717		
	25	–2.607		
PFeS&PEB	35	–2.724	12.152	1.016
	45	–2.851		
	25	–2.647		
PFeS&WAB	35	–2.782	12.773	1.157
	45	–2.903		

The enthalpy change (ΔH) > 0 demonstrated that the adsorption process was endothermic. Previous studies reported that when ΔH value was close to 2.1~20.9 kJ·mol^{-1}, the reaction belonged to physical adsorption, while, when the value was between 80 and 200 kJ·mol^{-1}, the reaction type was chemisorption [73]. Therefore, the ΔH values of PEB, WAB, PFeS&PEB and PFeS&WAB were all in the range of 2.1~20.9 kJ·mol^{-1}, while the value of Powder-FeS was closer to 20.9 kJ·mol^{-1}, indicating that the reaction process was more inclined to physical adsorption. Entropy change (ΔS) represented the degree of solid-liquid level disorder. Positive ΔS indicated an affinity between the adsorbent and Pb(II). During the adsorption process, the adsorption interface became more random and disorder increased. Studies showed that $\Delta S > 0$ and $\Delta H > 0$, the hydrophobic effect was the dominant force in the adsorption process [74]. Therefore, electrostatic attraction played an important role in the adsorption of Pb(II).

3.4. Reusability of PFeS&WAB and PFeS&PEB

Reusability was one of the important indexes to evaluate the economy and efficiency of materials in practical application [75,76]. Therefore, the recovery and regeneration performance of the adsorbent were particularly important. Reusability studies of PFeS&WAB and PFeS&PEB were eluting 0.1 M HNO_3. After four elutions, the removal efficiencies of PFeS&WAB and PFeS&PEB ranged from 36.367%, 31.153% to 35.963%, 30.653%, respectively (Fig. 8a). Meanwhile, no obvious variation of XRD patterns of the original biochar and the recycled biochar was observed (Fig. S1, the detailed of XRD comparison was in the supporting information). The results showed that PFeS&WAB and PFeS&PEB had good stability with the potential to remove Pb(II) in wastewater in practical application.

3.5. Adsorption mechanism

Based on the characterization results (SEM, EDS, BET, FTIR, XRD and XPS) and adsorption experiments (Figs. 5 and 7), the possible adsorption mechanism of Pb(II) removal from the solution by PFeS&WAB and PFeS&PEB is shown in Fig. 8b. BET data (Table S1) show that PFeS&WAB and PFeS&PEB had large specific surface areas and abundant pore structures, which provided sufficient physical adsorption sites for effective Pb adsorption (Fig. 8b, physical adsorption) [77]. FeS in PFeS&WAB and PFeS&PEB were excellent electron suppliers, which reduced Pb(II) in solution to Pb precipitation. At the same time, S(-II) and SO_4^{2-} (oxidation of S(-II)) formed precipitation (PbS and $PbSO_4$) with Pb(II) and separated from the solution (Fig. 8b), Oxidation–reduction reactions) [13]. EDS spectrum (Fig. 2) shows that there were other metal cations (such as K, Mg and Ca) on PFeS&WAB and PFeS&PEB surfaces that dissociated in solution, and Pb(II) occupied this position and adsorbed to the adsorbent surface, resulting in ion exchange (Fig. 8b, ion exchange) [78,79]. Both XRD, FTIR and XPS (Figs. 3 and 4) confirmed the existence of oxygen-containing functional groups (such as –COOH and –OH) in PFeS&WAB and PFeS&PEB. These oxygen-containing functional groups dissociated so that adsorbents surfaces became negatively charged and attracted the positively charged Pb(II) in solution electrostatically (Fig. 8b, electrostatic attraction) [13]. In addition, the complex reaction between oxygen-containing functional groups and Pb(II) formed hydrogen bonds to immobilize Pb(II) (Fig. 8b, complexation) [57]. Therefore, the removal of Pb(II) by PFeS&WAB and PFeS&PEB was the result of physical adsorption, oxidation-reduction reactions, ion exchange, complexation and electrostatic attraction.

3.6. Regression model analysis

As shown in Table 3, there were significant differences in pH, initial concentration and contact time ($p < 0.05$); Both pH and contact time had positive linear effect and negative squared terms, indicating that the change curves of Pb(II) with time and pH were quadratic-linear upward concave curves. That means they had a peak and then they

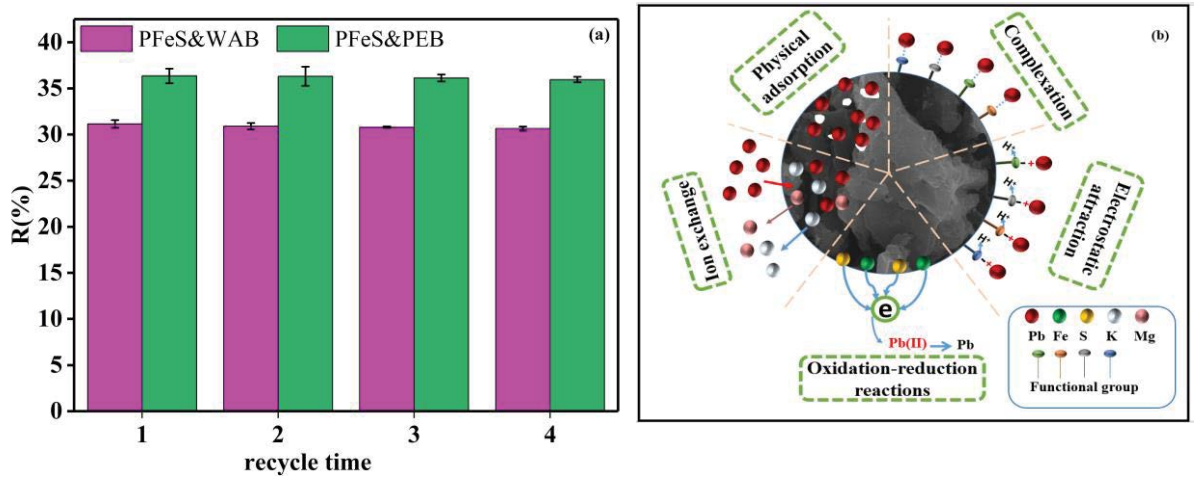

Fig. 8. Reusability of PFeS&WAB and PFeS&PEB for removing Pb(II) in solution (a) and the proposed reaction mechanism for the capture of Pb(II) (b).

Table 3
The *t*-statistics and *p*-values for coefficients of a pure-quadratic model

Parameter	Beta	SE	*t*-stat	*p*-value	Effect
Constant	34.241	10.863	3.042	0.002	Significant
pH	18.762	4.657	–3.877	0.003	Significant
C_0	–0.386	0.743	–4.863	0.000	Significant
Dosage	0.364	0.504	0.839	0.796	Insignificant
Time	0.449	0.098	5.643	0.000	Significant
pH^2	–1.383	0.472	–3.467	0.006	Significant
C_0^2	0.001	0.000	3.177	0.005	Significant
$Dosage^2$	–0.003	0.019	–0.164	0.498	Insignificant
$Time^2$	–0.006	0.000	–4.252	0.001	Significant

Model accuracy: $R^2 = 0.89$ and adjusted-$R^2 = 0.85$.

Table 4
Estimate adsorbent cost on kg scale

Raw materials used for adsorption	Unit price ($\$ kg^{-1}$)	Amount (kg)	Cost ($)
Walnut shells	0.1500	0.600	0.090
Peanut shells	0.05	0.600	0.030
H_2O	0.2500	5.000×10^{-2}	0.013
FeS	2.25	0.50	1.125
Cost of energy-consuming during heat treatment (Calcination + drying) ($)			0.430
Estimated total cost of the raw materials used for adsorption ($)			1.658
			1.598

went down [18]. In addition, the initial concentration had negative linear effect and positive squared terms, showing a quadratic convex type [36,78]. Meanwhile, the determination coefficient of pure quadratic equation (R^2) was 0.89, indicating that this model can well explain the variability of Pb(II) removal rate. After adjustment, the adjusted-R^2 was close to R^2, indicating that the model variables greatly affected the dependent variable, and the measured variables of the model were meaningful.

3.7. Cost analysis

The treatment of heavy metal polluted wastewater with low-cost adsorbents has been pursued by many researchers. The cost analysis study has also become a crucial indicator for evaluating and estimating the price of PFeS&WAB and PFeS&PEB, which makes it possible to compare the adsorption study with other wastewater treatment methods lead-containing wastewater. Therefore, the costs of PFeS&WAB and PFeS&PEB materials were calculated according to the methods already reported in the study [72,80,81]. Table 4 showed that the cost of prepared 1 kg of PFeS&WAB and PFeS&PEB was $1.658 and $1.598, respectively. It had a lower cost input than other adsorption materials (graphene oxide: $3.31 g, activated carbons: $ 2.6 kg, silica gels: $4.4~5.3 kg) [72]. Therefore, PFeS&WAB and PFeS&PEB have low preparation cost, environmentally benign characteristics and great potential to treat heavy metal polluted wastewater.

4. Conclusions

Two new biochars (PFeS&WAB and PFeS&PEB) were firstly synthesized from peanut shells biochar and walnut shells biochar, respectively. Their surface characteristics were improved by Powder-FeS modification to evaluate their batch adsorption potential for Pb(II) removal from wastewater. PFeS&PEB had the maximum adsorption capacity (98.039 $mg \cdot g^{-1}$). The adsorption process was mainly controlled by chemical reaction and monolayer absorption. The main adsorption mechanisms of Pb(II) were electrostatic attraction, ion exchange and REDOX reaction. In addition, PFeS&WAB and PFeS&PEB had the advantages of low preparation costs, high reusability and stability. Therefore, the novel biochars of PFeS&WAB and PFeS&PEB could be used as the biomaterials for effectively removing Pb(II) from wastewater in practical application.

Acknowledgement

This research was supported by the Joint Funds of the Zhejiang Provincial Natural Science Foundation of China under Grant No. LZY21C030001.

References

[1] H.A. Albert, X. Li, P. Jeyakumar, L. Wei, L. Huang, Q. Huang, M. Kamran, S.M. Shaheen, D. Hou, J. Rinklebe, Z. Liu, H. Wang, Influence of biochar and soil properties on soil and plant tissue concentrations of Cd and Pb: a meta-analysis, Sci. Total Environ., 755 (2021) 142582, doi: 10.1016/j.scitotenv.2020.142582.
[2] Y. Yang, F. Sun, J. Li, J. Chen, M. Tang, The effects of different factors on the removal mechanism of Pb(II) by biochar-supported carbon nanotube composites, RSC Adv., 10 (2020) 5988–5995.
[3] T. Zhou, Z. Wang, P. Christie, L. Wu, Cadmium and lead pollution characteristics of soils, vegetables and human hair around an open-cast lead-zinc mine, Bull. Environ. Contam. Toxicol., 107 (2021) 1176–1183.
[4] M.P. Taylor, C.F. Isley, J. Glover, Prevalence of childhood lead poisoning and respiratory disease associated with lead smelter emissions, Environ. Int., 127 (2019) 340–352.
[5] Z. Tao, Q. Guo, R. Wei, X. Dong, X. Han, Z. Guo, Atmospheric lead pollution in a typical megacity: evidence from lead isotopes, Sci. Total Environ., 778 (2021) 145810, doi: 10.1016/j.scitotenv.2021.145810.
[6] Y. Yan, F. Qi, S. Zhao, Y. Luo, S. Gu, Q. Li, L. Zhang, S. Zhou, N. Bolan, A new low-cost hydroxyapatite for efficient immobilization of lead, J. Colloid Interface Sci., 553 (2019) 798–804.
[7] C. Nzediegwu, S. Prasher, E. Elsayed, J. Dhiman, A. Mawof, R. Patel, Effect of biochar on heavy metal accumulation in potatoes from wastewater irrigation, J. Environ. Manage., 232 (2019) 153–164.
[8] Q. Chen, Y. Yao, X. Li, J. Lu, J. Zhou, Z. Huang, Comparison of heavy metal removals from aqueous solutions by chemical precipitation and characteristics of precipitates, J. Water Process Eng., 26 (2018) 289–300.
[9] Z. Han, Y. Guo, W. Yang, R. Tang, H. Wang, S. Wu, Removal of mercury from flue gases over iron modified activated carbon made by in situ ion exchange method, J. Energy Inst., 93 (2020) 1411–1418.

[10] K.N. Wahyusi, L.I. Utami, S. Aprilio, N. Fergina, Reduction of Pb and Cr levels in paper industrial liquid waste with ion exchange method, J. Phys.: Conf. Ser., 1569 (2020) 042054, doi: 10.1088/1742-6596/1569/4/042054.
[11] P. Kongsune, S. Rattanapan, R. Chanajaree, The removal of Pb^{2+} from aqueous solution using mangosteen peel activated carbon: isotherm, kinetic, thermodynamic and binding energy calculation, Groundwater Sustainable Dev., 12 (2021) 100524, doi: 10.1016/j.gsd.2020.100524.
[12] T.K. Tran, K.F. Chiu, C.Y. Lin, H.J. Leu, Electrochemical treatment of wastewater: Selectivity of the heavy metals removal process, Int. J. Hydrogen Energy, 42 (2017) 27741–27748.
[13] R. Liu, Y. Zhang, B. Hu, H. Wang, Improved Pb(II) removal in aqueous solution by sulfide@biochar and polysaccharose-FeS@biochar composites: efficiencies and mechanisms, Chemosphere, 287 (2022) 132087, doi: 10.1016/j.chemosphere.2021.132087.
[14] Y.H. Zhang, R.R. Liu, L.Y. Tan, N.C. Yang, H. Wang, Adsorption of Pb(II) by montmorillonite modified biochars and reduction Pb(II)-stress in plants of microcosms of constructed wetlands: mechanism and treatment performances, Desal. Water Treat., 221 (2021) 152–162.
[15] G. El Mouhri, M. Merzouki, H. Belhassan, Y. Miyah, H. Amakdouf, R. Elmountassir, A. Lahrichi, Continuous adsorption modeling and fixed bed column studies: adsorption of tannery wastewater pollutants using beach sand, J. Chem., 2020 (2020) 7613484, doi: 10.1155/2020/7613484.
[16] N. Loubna, Y. Miyah, F. Mejbar, M. Benjelloun, A. Ouissal, Y. Fahoul, V. Nenov, F. Zerrouq, Assessment of Brilliant Green and Eriochrome Black T dyes adsorption onto fava bean peels: kinetics, isotherms and regeneration study, Desal. Water Treat., 245 (2022) 255–269.
[17] S. Iaich, Y. Miyah, F. Azhar, S. Lagdali, M. Habacha, Low-cost ceramic microfiltration membranes made from Moroccan clay for domestic wastewater and Congo Red dye treatment, Desal. Water Treat., 235 (2021) 1–21.
[18] M. Fawzy, M. Nasr, S. Adel, S. Helmi, Regression model, artificial neural network, and cost estimation for biosorption of Ni(II)-ions from aqueous solutions by *Potamogeton pectinatus*, Int. J. Phytorem., 20 (2018) 321–329.
[19] G. El Mouhri, M. Merzouki, R. Kachkoul, H. Belhassan, Y. Miyah, H. Amakdouf, R. Elmountassir, A. Lahrichi, Fixed-bed adsorption of tannery wastewater pollutants using bottom ash: an optimized process, Surf. Interfaces, 22 (2021) 100868, doi: 10.1016/j.surfin.2020.100868.
[20] M. Benjelloun, Y. Miyah, G. Akdemir Evrendilek, F. Zerrouq, S. Lairini, Recent advances in adsorption kinetic models: their application to dye types, Arabian J. Chem., 14 (2021) 103031, doi: 10.1016/j.arabjc.2021.103031.
[21] Y. Shi, R. Shan, L. Lu, H. Yuan, H. Jiang, Y. Zhang, Y. Chen, High-efficiency removal of Cr(VI) by modified biochar derived from glue residue, J. Cleaner Prod., 254 (2020) 119935, doi: 10.1016/j.jclepro.2019.119935.
[22] L. Liu, X. Liu, D. Wang, H. Lin, L. Huang, Removal and reduction of Cr(VI) in simulated wastewater using magnetic biochar prepared by co-pyrolysis of nano-zero-valent iron and sewage sludge, J. Cleaner Prod., 257 (2020) 120562, doi: 10.1016/j.jclepro.2020.120562.
[23] Z. Ding, X. Hu, A.R. Zimmerman, B. Gao, Sorption and cosorption of lead(II) and methylene blue on chemically modified biomass, Bioresour. Technol., 167 (2014) 569–573.
[24] Y.H. Li, S. Wang, J. Wei, X. Zhang, C. Xu, Z. Luan, D. Wu, B. Wei, Lead adsorption on carbon nanotubes, Chem. Phys. Lett., 357 (2002) 263–266.
[25] R. Li, H. Deng, X. Zhang, J.J. Wang, M.K. Awasthi, Q. Wang, R. Xiao, B. Zhou, J. Du, Z. Zhang, High-efficiency removal of Pb(II) and humate by a CeO_2–MoS_2 hybrid magnetic biochar, Bioresour. Technol., 273 (2019) 335–340.
[26] S. Wang, S. Bian, J. Liu, J. Li, S. Xu, Z. Liang, Highly adsorptive pristine and magnetic biochars prepared from crayfish shell for removal of Cu(II) and Pb(II), J. Taiwan Inst. Chem. Eng., 127(2021) 175–185.
[27] T. Liu, B. Gao, J. Fang, B. Wang, X. Cao, Biochar-supported carbon nanotube and graphene oxide nanocomposites for Pb(II) and Cd(II) removal, RSC Adv., 6 (2016) 24314–24319.
[28] A. Mitzia, M. Vítková, M. Komárek, Assessment of biochar and/or nano zero-valent iron for the stabilisation of Zn, Pb and Cd: a temporal study of solid phase geochemistry under changing soil conditions, Chemosphere, 242 (2020) 125248, doi: 10.1016/j.chemosphere.2019.125248.
[29] F. Yang, S. Zhang, Y. Sun, K. Cheng, J. Li, D.C.W. Tsang, Fabrication and characterization of hydrophilic corn stalk biochar-supported nanoscale zero-valent iron composites for efficient metal removal, Bioresour. Technol., 265 (2018) 490–497.
[30] H. Wang, Q. Chen, R.R. Liu, Y.C. Zhang, Y.H. Zhang, Synthesis and application of starch-stablized Fe–Mn/biochar composites for the removal of lead from water and soil, Chemosphere, 305 (2022) 135494, doi: 10.1016/j.chemosphere.2022.135494.
[31] S. Cheng, B. Xing, C. Shi, Y. Nie, H. Xia, Efficient and selective removal of Pb(II) from aqueous solution by modification crofton weed: experiment and density functional theory calculation, J. Cleaner Prod., 280 (2021) 124407, doi: 10.1016/j.jclepro.2020.124407.
[32] A. Lu, S. Zhong, J. Chen, J. Shi, J. Tang, X. Lu, Removal of Cr(VI) and Cr(III) from aqueous solutions and industrial wastewaters by natural clino-pyrrhotite, Environ. Sci. Technol., 40 (2006) 3064–3069.
[33] E. Sathiyaraj, S. Thirumaran, S. Ciattini, S. Selvanayagam, Synthesis and characterization of Ni(II) complexes with functionalized dithiocarbamates: new single source precursors for nickel sulfide and nickel-iron sulfide nanoparticles, Inorg. Chim. Acta, 498 (2019) 119162, doi: 10.1016/j.ica.2019.119162.
[34] X. Wei, H. Yin, H. Peng, R. Chen, G. Lu, Z. Dang, Reductive debromination of decabromodiphenyl ether by iron sulfide-coated nanoscale zerovalent iron: mechanistic insights from Fe(II) dissolution and solvent kinetic isotope effects, Environ. Pollut., 253 (2019) 161–170.
[35] H. Wu, L. Li, K. Chang, K. Du, C. Shen, S. Zhou, G. Sheng, W. Linghu, T. Hayat, X. Guo, Graphene oxide decorated nanoscale iron sulfide for highly efficient scavenging of hexavalent chromium from aqueous solutions, J. Environ. Chem. Eng., 8 (2020) 103882, doi: 10.1016/j.jece.2020.103882.
[36] A. Hamdy, M.K. Mostafa, M. Nasr, Regression analysis and artificial intelligence for removal of methylene blue from aqueous solutions using nanoscale zero-valent iron, Int. J. Environ. Sci. Technol., 16 (2019) 357–372.
[37] J. Liu, K.T. Valsaraj, I. Devai, R.D. DeLaune, Immobilization of aqueous Hg(II) by mackinawite (FeS), J. Hazard. Mater., 157 (2008) 432–440.
[38] M.Y. Yen, C.C. Teng, M.C. Hsiao, P.I. Liu, W.P. Chuang, C.C.M. Ma, C.K. Hsieh, M.C. Tsai, C.H. Tsai, Platinum nanoparticles/graphene composite catalyst as a novel composite counter electrode for high performance dye-sensitized solar cells, J. Mater. Chem., 21 (2011) 12880–12888.
[39] X. Zhang, Y. Yang, S. Guo, F. Hu, L. Liu, Mesoporous $Ni_{0.85}Se$ nanospheres grown in situ on graphene with high performance in dye-sensitized solar cells, ACS Appl. Mater. Interfaces, 7 (2015) 8457–8464.
[40] R. Melhaoui, Y. Miyah, S. Kodad, N. Houmy, M. Addi, M. Abid, A. Mihamou, H. Serghini-Caid, S. Lairini, N. Tijani, C. Hano, A. Elamrani, On the suitability of almond shells for the manufacture of a natural low-cost bioadsorbent to remove brilliant green: kinetics and equilibrium isotherms study, Sci. World J., 2021 (2021) 6659902, doi: 10.1155/2021/6659902.
[41] Y. Yang, Y. Zhang, G. Wang, Z. Yang, J. Xian, Y. Yang, T. Li, Y. Pu, Y. Jia, Y. Li, Z. Cheng, S. Zhang, X. Xu, Adsorption and reduction of Cr(VI) by a novel nanoscale FeS/chitosan/biochar composite from aqueous solution, J. Environ. Chem. Eng., 9 (2021) 105407, doi: 10.1016/j.jece.2021.105407.
[42] D. Xu, J. Cao, Y. Li, A. Howard, K. Yu, Effect of pyrolysis temperature on characteristics of biochars derived from different feedstocks: a case study on ammonium adsorption capacity, Waste Manage., 87 (2019) 652–660.

[43] M.B. Ahmed, J.L. Zhou, H.H. Ngo, W. Guo, M.A.H. Johir, K. Sornalingam, D. Belhaj, M. Kallel, Nano-Fe^0 immobilized onto functionalized biochar gaining excellent stability during sorption and reduction of chloramphenicol via transforming to reusable magnetic composite, Chem. Eng. J., 322 (2017) 571–581.
[44] W. Wu, M. Yang, Q. Feng, K. McGrouther, H. Wang, H. Lu, Y. Chen, Chemical characterization of rice straw-derived biochar for soil amendment, Biomass Bioenergy, 47 (2012) 268–276.
[45] Q. Hong, C. Liu, Z. Wang, R. Li, X. Liang, Y. Wang, Y. Zhang, Z. Song, Z. Xiao, T. Cui, B. Heng, B. Xu, F. Qi, A. Ikhlaq, Electron transfer enhancing Fe(II)/Fe(III) cycle by sulfur and biochar in magnetic FeS@biochar to active peroxymonosulfate for 2,4-dichlorophenoxyacetic acid degradation, Chem. Eng. J., 417 (2021) 129238, doi: 10.1016/j.cej.2021.129238.
[46] X. Chen, X. Wang, D. Fang, A review on C1s XPS-spectra for some kinds of carbon materials, Fullerenes Nanotubes Carbon Nanostruct., 28 (2020) 1048–1058.
[47] W. Zhang, J. Li, P. Guan, C. Lv, C. Yang, N. Han, X. Wang, G. Song, Z. Peng, One-pot sol-gel synthesis of Si/C yolk-shell anodes for high performance lithium-ion batteries, J. Alloys Compd., 835 (2020) 155135, doi: 10.1016/j.jallcom.2020.155135.
[48] D. Mu, Z. Chen, H. Shi, N. Tan, Construction of flower-like MoS_2/Fe_3O_4/rGO composite with enhanced photo-Fenton like catalyst performance, RSC Adv., 8 (2018) 36625–36631.
[49] N. Pachauri, G.B.V.S. Lakshmi, S. Sri, P.K. Gupta, P.R. Solanki, Silver molybdate nanoparticles based immunosensor for the non-invasive detection of Interleukin-8 biomarker, Mater. Sci. Eng., C, 113 (2020) 110911, doi: 10.1016/j.msec.2020.110911.
[50] C. Wei, S. Hu, F. Liang, Z. Song, X. Liu, One-pot synthesis of concentration and excitation dual-dependency truly full-color photoluminescence carbon dots, Chin. Chem. Lett., 33 (2022) 4116–4120.
[51] R. Al-Gaashani, B. Aïssa, M. Anower Hossain, S. Radiman, Catalyst-free synthesis of ZnO-CuO-$ZnFe_2O_4$ nanocomposites by a rapid one-step thermal decomposition approach, Mater. Sci. Semicond. Process., 90 (2019) 41–49.
[52] K. Carrera, V. Huerta, V. Orozco, J. Matutes, P. Fernández, O.A. Graeve, M. Herrera, Formation of vacancy point-defects in hydroxyapatite nanobelts by selective incorporation of Fe^{3+} ions in Ca(II) sites. A CL and XPS study, Mater. Sci. Eng., B, 271 (2021) 115308, doi: 10.1016/j.mseb.2021.115308.
[53] C.C. Wang, S. Darvish, K. Chen, B. Hou, Q. Zhang, Z. Tan, Y. Zhong, S.P. Jiang, Combined Cr and S poisoning of $La_{0.8}Sr_{0.2}MnO_{3-\delta}$ (LSM) cathode of solid oxide fuel cells, Electrochim. Acta, 312 (2019) 202–212.
[54] M. Zhu, G. Wang, X. Liu, B. Guo, G. Xu, Z. Huang, M. Wu, H.K. Liu, S.X. Dou, C. Wu, Dendrite-free sodium metal anodes enabled by a sodium benzenedithiolate-rich protection layer, Angew. Chem. Int. Ed., 59 (2020) 6596–6600.
[55] J. Liu, W. Kong, Z. Jin, Y. Han, J. Sun, L. Ma, Y. Niu, Y. Xu, A MoFe nitrogenase-mimicking electrocatalyst for nitrogen fixation with high faradaic efficiency, J. Mater. Chem. A, 8 (2020) 19278–19282.
[56] M. Chen, D. Liu, B. Zi, Y. Chen, D. Liu, X. Du, F. Li, P. Zhou, Y. Ke, J. Li, K.H. Lo, C.T. Kwok, W.F. Ip, S. Chen, S. Wang, Q. Liu, H. Pan, Remarkable synergistic effect in cobalt-iron nitride/alloy nanosheets for robust electrochemical water splitting, J. Energy Chem., 65 (2022) 405–414.
[57] H. Wang, R. Liu, Q. Chen, Y. Mo, Y. Zhang, Biochar-supported starch/chitosan-stabilized nano-iron sulfide composites for the removal of lead ions and nitrogen from aqueous solutions, Bioresour. Technol., 347 (2022) 126700, doi: 10.1016/j.biortech.2022.126700.
[58] J. Lu, B. Zhang, C. He, A.G.L. Borthwick, The role of natural Fe(II)-bearing minerals in chemoautotrophic chromium(VI) bio-reduction in groundwater, J. Hazard. Mater., 389 (2020) 121911, doi: 10.1016/j.jhazmat.2019.121911.
[59] Y. Lan, Y. Huang, H. Qi, L. Lai, L. Xia, Z. Zhao, Y. Zhao, Alternating electric field-based ionic control and layer-by-layer assembly of anion exchange membranes for enhancing target anion selectivity, Desalination, 533 (2022) 115773, doi: 10.1016/j.desal.2022.115773.
[60] S. Azarkan, A. Peña, K. Draoui, C.I. Sainz-Díaz, Adsorption of two fungicides on natural clays of Morocco, Appl. Clay Sci.,123 (2016) 37–46.
[61] R.Z. Wang, D.L. Huang, Y.G. Liu, C. Zhang, C. Lai, G.M. Zeng, M. Cheng, X.-M. Gong, J. Wan, H. Luo, Investigating the adsorption behavior and the relative distribution of Cd^{2+} sorption mechanisms on biochars by different feedstock, Bioresour. Technol., 261 (2018) 265–271.
[62] R. Deng, H. Luo, D. Huang, C. Zhang, Biochar-mediated Fenton-like reaction for the degradation of sulfamethazine: role of environmentally persistent free radicals, Chemosphere, 255 (2020) 126975, doi: 10.1016/j.chemosphere.2020.126975.
[63] Q. Miao, G. Li, Potassium phosphate/magnesium oxide modified biochars: interfacial chemical behaviours and Pb binding performance, Sci. Total Environ., 759 (2021) 143452, doi: 10.1016/j.scitotenv.2020.143452.
[64] Y. Miyah, A. Lahrichi, M. Idrissi, S. Boujraf, H. Taouda, F. Zerrouq, Assessment of adsorption kinetics for removal potential of Crystal Violet dye from aqueous solutions using Moroccan pyrophyllite, J. Assoc. Arab Univ. Basic Appl. Sci., 23 (2017) 20–28.
[65] H. Paudyal, B. Pangeni, K. Nath Ghimire, K. Inoue, K. Ohto, H. Kawakita, S. Alam, Adsorption behavior of orange waste gel for some rare earth ions and its application to the removal of fluoride from water, Chem. Eng. J., 195–196 (2012) 289–296.
[66] R. Deng, D. Huang, G. Zeng, J. Wan, W. Xue, X. Wen, X. Liu, S. Chen, J. Li, C. Liu, Q. Zhang, Decontamination of lead and tetracycline from aqueous solution by a promising carbonaceous nanocomposite: interaction and mechanisms insight, Bioresour. Technol., 283 (2019) 277–285.
[67] S. Bakshi, D.A. Laird, R.G. Smith, R.C. Brown, Capture and release of orthophosphate by Fe-modified biochars: mechanisms and environmental applications, ACS Sustainable Chem. Eng., 9 (2021) 658–668.
[68] G.M. Shah, M. Nasir, M. Imran, H.F. Bakhat, F. Rabbani, M. Sajjad, A.B. Umer Farooq, S. Ahmad, L. Song, Biosorption potential of natural, pyrolysed and acid-assisted pyrolysed sugarcane bagasse for the removal of lead from contaminated water, PeerJ, 6 (2018) e5672, doi: 10.7717/peerj.5672.
[69] M. Imran, Z.U.H. Khan, M.M. Iqbal, J. Iqbal, N.S. Shah, S. Munawar, S. Ali, B. Murtaza, M.A. Naeem, M. Rizwan, Effect of biochar modified with magnetite nanoparticles and HNO_3 for efficient removal of Cr(VI) from contaminated water: a batch and column scale study, Environ. Pollut., 261 (2020) 114231, doi: 10.1016/j.envpol.2020.114231.
[70] T. Yang, Y. Xu, Q. Huang, Y. Sun, X. Liang, L. Wang, X. Qin, L. Zhao, Adsorption characteristics and the removal mechanism of two novel Fe-Zn composite modified biochar for Cd(II) in water, Bioresour. Technol., 333 (2021) 125078, doi: 10.1016/j.biortech.2021.125078.
[71] Y. Li, F. Wang, Y. Miao, Y. Mai, H. Li, X. Chen, J. Chen, A lignin-biochar with high oxygen-containing groups for adsorbing lead ion prepared by simultaneous oxidization and carbonization, Bioresour. Technol., 307 (2020) 123165, doi: 10.1016/j.biortech.2020.123165.
[72] M. Benjelloun, Y. Miyah, R. Bouslamti, L. Nahali, F. Mejbar, S. Lairini, The fast-efficient adsorption process of the toxic dye onto shells powders of walnut and peanut: experiments, equilibrium, thermodynamic, and regeneration studies, Chem. Afr., 5 (2022) 375–393.
[73] R.M. de Souza, H.B. Quesada, L.F. Cusioli, M.R. Fagundes-Klen, R. Bergamasco, Adsorption of non-steroidal anti-inflammatory drug (NSAID) by agro-industrial by-product with chemical and thermal modification: adsorption studies and mechanism, Ind. Crops Prod., 161 (2021) 113200, doi: 10.1016/j.indcrop.2020.113200.
[74] L. Joseph, V.P. Sylas, N. Cyril, K.S. Sanu, S. Jose, B.N. Anila, J.M. Jose, Removal of endrin from aqueous medium using Accacia wood biochar: kinetics and thermodynamic

studies, Biomass Convers. Biorefin., (2021), doi: 10.1007/s13399-021-01435-8.
[75] Y. Miyah, A. Lahrichi, R. Kachkoul, G. El Mouhri, M. Idrissi, S. Iaich, F. Zerrouq, Multi-parametric filtration effect of the dyes mixture removal with the low cost materials, Arab J. Basic Appl. Sci., 27 (2020) 248–258.
[76] Y. Miyah, A. Lahrichi, M. Idrissi, A. Khalil, F. Zerrouq, Adsorption of methylene blue dye from aqueous solutions onto walnut shells powder: equilibrium and kinetic studies, Surf. Interfaces, 11 (2018) 74–81.
[77] M.I. Inyang, B. Gao, Y. Yao, Y. Xue, A. Zimmerman, A. Mosa, P. Pullammanappallil, Y.S. Ok, X. Cao, A review of biochar as a low-cost adsorbent for aqueous heavy metal removal, Crit. Rev. Env. Sci. Technol., 46 (2016) 406–433.
[78] M. Fawzy, M. Nasr, A.M. Abdel-Rahman, G. Hosny, B.R. Odhafa, Techno-economic and environmental approaches of Cd^{2+} adsorption by olive leaves (*Olea europaea* L.) waste, Int. J. Phytorem., 21 (2019) 1205–1214.
[79] M.K. Nayunigari, S.K. Gupta, M. Nasr, G. Andaluri, R.P.S. Suri, A. Maity, Artificial neural network and cost estimation for Cr(VI) removal using polycationic composite adsorbent, Water Environ. J., 34 (2020) 29–40.
[80] Y. Miyah, M. Benjelloun, A. Lahrichi, F. Mejbar, S. Iaich, G. El Mouhri, R. Kachkoul, F. Zerrouq, Highly-efficient treated oil shale ash adsorbent for toxic dyes removal: kinetics, isotherms, regeneration, cost analysis and optimization by experimental design, J. Environ. Chem. Eng., 9 (2021) 106694, doi: 10.1016/j.jece.2021.106694.
[81] Y. Miyah, M. Benjelloun, R. Salim, L. Nahali, F. Mejbar, A. Lahrichi, S. Iaich, F. Zerrouq, Experimental and DFT theoretical study for understanding the adsorption mechanism of toxic dye onto innovative material Fb-HAp based on fishbone powder, J. Mol. Liq., 362 (2022) 119739, doi: 10.1016/j.molliq.2022.119739.

Supporting information

S1. Adsorption experiments

All adsorption experiments were carried out in a 250 mL conical flask with a solution volume of 100 mL and agitated at 200 rpm for 270 min at a constant temperature of 25°C ± 1°C. Except for the pH test, the initial pH of the solution is adjusted to 5 ± 0.1 with 1 M NaOH and 1 M HCl. The concentration of Pb(II) was 60 mg·L^{-1} except for the experiment of isothermal initial concentration. The dosage of adsorbent was 0.75 g·L^{-1} (except the dosage experiment). After the adsorption experiment, the supernatant containing Pb(II) was filtered through 0.45 um membrane. Then the concentration of Pb(II) was determined by UV-Vis spectrophotometry.

In order to explore the influence of initial pH on the adsorption performance of Pb(II), 1 M of NaOH or HCl was used to adjust pH to 2, 3, 4, 5, 6 and 7. To study the influence of different initial concentration of Pb(II) on adsorption performance, the concentration of Pb(II) was adjusted to 20, 40, 60, 80 and 100 mg·L^{-1}, respectively. To determine the equilibrium time of adsorbents, samples were taken at 5, 10, 15, 30, 60, 90, 150, 210 and 270 min. The dosage of adsorbent was set as 0.25, 0.5, 0.75, 1 and 1.25 g·L^{-1}, to explore the effect of dosage on adsorption performance.

The removal rate (R) and the removal capacity (q_e) was calculated using Eqs. (S1) and (S2).

$$R = \frac{\left(C_0 - C_e\right)}{C_0} \times 100 \tag{S1}$$

$$q_e = \frac{\left(C_0 - C_e\right) \times V}{m} \tag{S2}$$

where C_0 (mg·L^{-1}) and C_e (mg·L^{-1}) were the initial concentration and equilibrium concentration, respectively. V (L) was the solution volume, and m (g) was the weight of the adsorbent.

S2. Determination of point of the zero charge

The determination of the pH of point of zero charge (PZC) of the biochars (PEB, WAB, Powder-FeS, PFeS&PEB, and PFeS&WAB) was carried out as follows: a series of 150 mL 0.1 M NaCl solution in a conical flask with a stopper. All the solutions were added N_2 for 5 min to remove CO_2. The initial pH ($pH_{initial}$) of the solution was adjusted to 2–10 with 0.1 M HCl or 0.1 M NaOH. Then, 0.6 g biochar was added to the glass tube. The final pH (pH_{final}) was measured after 24 h oscillation at 200 rpm, at 25°C. pH_{PZC} was determined by the initial pH and final pH. ΔpH was the $pH_{initial}$ minus the pH_{final}. ΔpH > 0 indicated that the adsorbent surface had a positive charge, ΔpH < 0 with a negative charge, ΔpH = 0 was the point of zero charge (PZC).

S3. Adsorption kinetics, adsorption isotherm and thermodynamics

Pseudo-first kinetic model and pseudo-second kinetic model were as follows:

$$q_t = q_e\left(1 - e^{-k_1 t}\right) \tag{S3}$$

$$q_t = \frac{k_2 q_e^2 t}{1 + k_2 q_e t} \tag{S4}$$

where q_t (mg·g^{-1}) was the adsorbed amount of Pb(II) at a certain time; q_e (mg·g^{-1}) was the adsorption capacityof equilibrium; k_1 (min^{-1}) was the adsorption rate constant of pseudo-first kinetic model; k_2 (g(mg·min)$^{-1}$) was the adsorption rate constant of pseudo-second kinetic model.

The adsorption equations of L-model (S5) and F-model (S6) were as follows:

$$\frac{1}{q_e} = \frac{1}{q_{\max}} + \frac{1}{q_{\max} K_L C_e} \tag{S5}$$

Table S1
Structural parameters of the PEB, WAB, PFeS&PEB and PFeS&WAB

Samples	S_{BET}	Pore size	Pore volume
	$m^2 \cdot g^{-1}$	nm	$cm^3 \cdot g^{-1}$
PEB	8.07	12.96	0.104
WAB	7.19	19.43	0.191
PFeS&PEB	51.14	8.57	0.082
PFeS&WAB	46.49	10.86	0.099

Specific surface area (S_{BET}).

$$\ln q_e = \ln K_F + \frac{1}{n}\ln C_e \quad \text{(S6)}$$

where q_{max} (mg·g^{-1}) was maximum adsorption calculated by L-model; K_L (L·mg^{-1}) was equilibrium constant for L-model; C_e (mg·L^{-1}) was the concentration of Pb(II) at equilibrium. K_F was the F-model constant; n was dimensionless constant to reflect the adsorption strength.

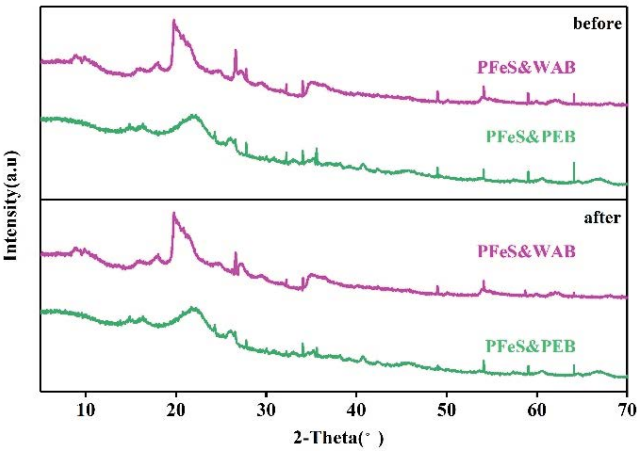

Fig. S1. XRD patterns of the original biochar (before) and the recycled biochar (after) of Pb(II).

To further investigate the influence of temperature on Pb(II) removal efficiency of adsorbent, Gibbs free energy (ΔG), enthalpy change (ΔH) and entropy change (ΔS) in Pb(II) adsorption process were calculated by the following equations:

$$\Delta G = -RT\ln K_D \quad \text{(S7)}$$

$$\ln K_D = \frac{-\Delta H}{RT} = \frac{\Delta S}{R} \quad \text{(S8)}$$

$$K_D = \frac{q_e}{c_e} \quad \text{(S9)}$$

where R (8.314 J·mol^{-1}·K^{-1}) was the molar gas constant; T (K) was the reaction temperature.

S4. X-ray diffraction comparison before and after adsorption

After adsorption, the biochar was washed with 0.1 M HNO_3 for several times to obtain the recycled biochar. The X-ray diffraction (XRD) patterns of the original biochar (before) and the recycled biochar (after) were shown in Fig. S1. No significant changes were found in XRD spectra before and after adsorption (Fig. S1). It indicated that stability and reusability of PFeS&PEB and PFeS&WAB was good.